Temporal Change of Stress Tensors and Gutenberg—Richter's b Value during the Aftershock Sequence following the Kameoka Earthquake (1987, M=4.9) in Southwestern Japan

AUTHOR(S):

MAEDA, Naoki; WATANABE, Hikaru

Bull. Disas. Prev. Res. Inst., Kyoto Univ., Vol. 41, Part 1, No. 353, March, 1991

Temporal Change of Stress Tensors and Gutenberg–Richter's b Value during the Aftershock Sequence following the Kameoka Earthquake (1987, M=4.9) in Southwestern Japan

By Naoki MAEDA and Hikaru WATANABE

(Manuscript received on February 5, 1991)

Abstract

A relation between the temporal change of the stress tensors estimated using focal mechanisms and the temporal change of Gutenberg–Richter's b value which had been related to differential stress or heterogeneity of medium, was investigated for the aftershock sequence following the Kameoka earthquake (M=4.9), which occurred on May 28, 1987 in the midst of the seismic network of the Abuyama Seismological Observatory, Kyoto University. The main purpose of this study is to obtain information on the state of the stress during the aftershock sequence with a very high degree of accuracy.

As a result of the analysis, the rotation of the maximum principal axis of the stress was found. The rotation shows exponential change with a time constant of 14 days. It is revealed that this time constant is related to the period of the occurrence of the aftershocks with strike slip faulting or intermediate faulting types which are different from that of the main shock and that it is related also to the period where the modified Omori formula holds good.

The rotation of the maximum principal stress derived by using the stress tensor inversion has been reported for the aftershock sequences of the Coalinga earthquake (1983, M=6.7) by Michael (1987b) and the Oceanside earthquake (1986, M=5.3) by Hauksson and Jones (1988). The time constants deduced from their data were about 15 days for the Coalinga sequence and about 5 days for the Oceanside sequence. These values for the time constant seemed not to vary significantly with magnitude of earthquake.

As regards the temporal change of b value, meaningfully large values were found within five days after the main shock. In this period, the aftershocks were occurring in the region where the stress level was high. The fact that the large b values occurred under a small magnitude of stress level in the case of rock experiment, seemed not to hold for the aftershock sequence of the Kameoka earthquake.

1. Introduction

Information on the state of stress during a sequence of earthquakes can give us a clue to understanding the physical process of the sequence. In this study, the temporal change of the stress tensors estimated using focal mechanisms and the temporal change of Gutenberg–Richter's b values which had been related to differential stress or heterogeneity of medium from experimental results were investigated for the aftershock sequence following the Kameoka earthquake on May 28, 1987 (M=4.9). Small earthquakes with magnitude (M) of approximately 5 have a source dimension of about one kilometer, while earthquakes of M 6 to 7 have source dimensions of about ten kilometers. Small source dimensions along with small magnitudes require a high degree of accuracy in the

location of hypocenters and high detection capability for aftershocks. Furthermore, focal mechanisms of aftershocks are difficult to determine because the magnitudes of aftershocks are still smaller than that of the main shock. In this respect it was fortunate that the Kameoka earthquake occurred in the midst of the seismic network of the Abuyama Seismological Observatory (ASO) of Kyoto University. This network has an unusually dense concentration of seismic observing stations. Therefore, many an aftershock can be located with a sufficient degree of accuracy for the purpose of this study. In addition, Maeda (1988) designed a method for determining focal mechanisms for an earthquake cluster, where polarities (up and down) and amplitudes of P first motions were utilized together. We then applied it to the aftershock sequence following the Kameoka earthquake and successfully determined a lot of focal mechanisms of aftershocks.

Focal mechanisms give information on the direction of the principal stresses of the stress field. Aftershocks occur in regions where the stress field was severely disturbed by the coseismic slip of the main shock and weak planes could be newly generated during the main shock. Therefore, the individual focal mechanisms of aftershocks usually show various faulting types. A kind of averaging method of the focal mechanisms is necessary for obtaining the stress tensors. Michael (1987a) designed a method for estimating a stress tensor using the slip data of focal mechanisms. In the method by Michael (1987a), the linear inversion proposed earlier by him (1984) is carried out in order to obtain stress tensors. Using this method, we can obtain the stress tensors which give a similar value of tangential tractions on the fault plane derived from each of the data sets. Taking a fracture criterion, e. g., the Coulomb's fracture criterion into account, such an inversion method as described above seems to be preferable. In this paper, the temporal change of the stress tensors during the aftershock sequence following the Kameoka earthquake was calculated by using this method with some modifications in the step of fault plane choice.

The temporal change of Gutenberg–Richter's b value (Gutenberg and Richter, 1944) during the aftershock sequence was also investigated. The Gutenberg–Richter's b value has been related to the differential stress or to the heterogeneity of the medium from experimental results as follows. As differential stress becomes larger, b value becomes smaller (Scholz, 1968). As heterogeneity of the medium becomes larger, b value becomes larger (Mogi, 1962). Since aftershocks occur in regions where the stress field is severely disturbed due to main shock faulting, the changes of the magnitude of the stress and heterogeneity during the aftershock sequence are thought to be large. Therefore, making the comparison of the temporal change of b value with the temporal change of the stress tensor or the temporal change of the active region of the aftershocks, we may clarify the physical meaning of b value, that is, the relation between b value and the stress. From this point of view, the temporal change of b value during the aftershock sequence following the Kameoka earthquake was investigated by using very small aftershocks as low as magnitudes of 0.2.

The aftershock sequence following the Kameoka earthquake was profitably observed as outlined above. Using the data with a high degree of accuracy, we will study the state of the stress in regions where aftershocks occur and attempt to obtain clues to

understanding the mechanism of the occurrence of aftershocks.

2. Kameoka earthquake

2.1 Seismic network

In areas of Kyoto Prefecture, northern Osaka Prefecture, and western portions of Lake Biwa, numerous microearthquakes of M less than 4.0 occur (e. g., see Maeda and Watanabe, 1984). In order to investigate the seismicity of this region, microearthquake observations originated in 1962. A telemetered system was installed in 1975 by the Abuyama Seismological Observatory (ASO), Faculty of Science, Kyoto University (Kuroiso and Watanabe, 1977). For greater observational coverage, seismograms obtained from adjoing networks have been available since 1979 by means of the wave data exchange system among seismic networks of neighboring universities (Watanabe *et al.*, in preparation). The observation stations are shown in **Fig. 1.** Solid circles represent the ASO stations, while open circles represent the stations of the adjoining networks whose seismograms are available at ASO. Short-period and high-gain seismograms of the three components observed at the ASO stations and vertical components observed at the adjoining network stations are available at ASO. Short-period and high-gain seismographs have a natural period of 1 s. In addition, five stations, namely, ABU,

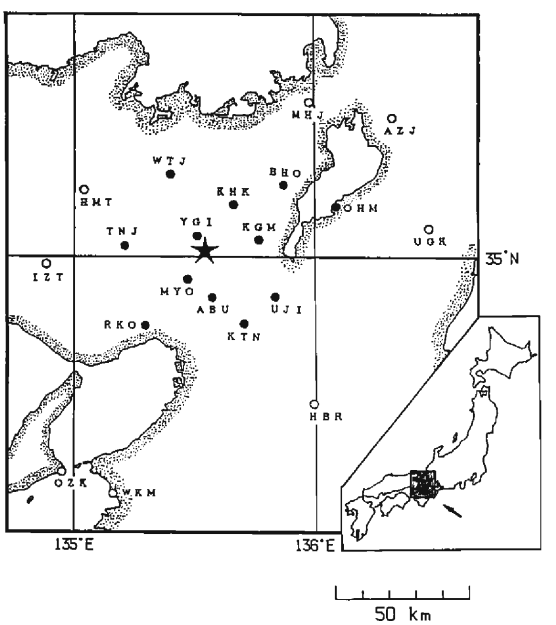

Fig. 1. Epicenter of the Kameoka earthquake and distribution of the observation stations. The star symbol represents the epicenter. Solid circles represent stations of telemetered network system of the Abuyama Seismological Observatory of Kyoto University. Open circles represent stations of the adjoining telemetered networks of other organizations, whose seismograms are available through the seismic wave exchanging system.

WTJ, UJI, KTN, and RKO, are equipped with medium-period and low-gain seismographs having a natural period of 10 s which measure vertical components.

2.2 Location of Kameoka earthquake

In the determination of the hypocenter of the main shock, use was made of the P times of 12 ASO stations and S times from ABU, UJI, KTN, and RKO which were picked from low-gain seismograms. The weighting factor for the S times in hypocenter determination was set at one tenth of that of the P times. The P wave velocity model used in this study has a horizontal layered struture, as shown in **Table 1.** In order to reduce the error in hypocenter determination further, we adopted a model with lateral variation of the thickness of the uppermost layer in **Table 1** after Maeda and Watanabe (1984). S wave velocities were simply calculated on the assumption that V_P/V_S is 1. 7.

Table 1. Parameters of the horizontally layered velocity model

layer	velocity (km/s)	thickness (km)
1	5.5	5.0
2	6.0	13.0
3	6.7	12.0
4	8.0	....

The main shock was located at $x=4.40$, $y=1.67$, and $z=12.1$ in the coordinate system used by ASO. Here x, y, and z are measured eastward, northward and downward, respectively, in units of km from the origin (35°N, 135°30′E, and sea level). The location of the epicenter of the main shock is shown by the star symbol in **Fig. 1.** The Kameoka earthquake occurring in the midst of the network, the hypocenter of the main shock was located with a very high degree of accuracy. Maeda (submitted) estimated the horizontal error and the vertical error in the location as 0.2 km and 0.9 km, at the most, respectively, taking the error in the P times and the error in the velocity model into account.

The focal mechanism was determined as shown in **Fig. 2.** The strike and dip of one nodal plane were N6°W and 41°W, and those of another plane were N15°W and 51°E.

2.3 Location of aftershocks

The location capability of the ASO network in the area of the hypocenter of Kameoka earthquake was estimated by Maeda (submitted), using the method found in Matsumura (1984). At ASO, earthquakes having four or more P times were located until June 1987, while earthquakes with six or more P times have been located since July 1987. **Fig. 3** shows the location capability curves versus the magnitude for these two criteria. More than 95% of earthquakes with magnitudes of 1.0 were located during the Kameoka aftershock sequence.

Aftershocks which occurred until 30 September 1987 were relocated using the modified master event technique (Ito and Kuroiso, 1979). Relocated hypocenters of aftershocks with magnitudes greater than or equal to 1.0 are shown in **Fig. 4.** As shown

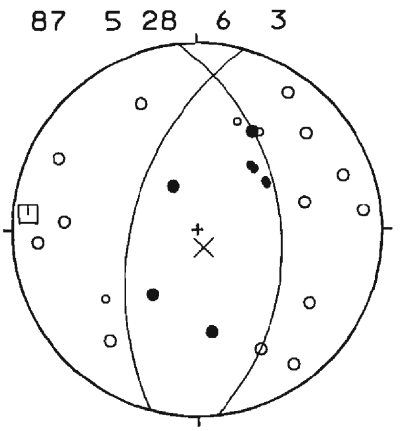

Fig. 2. Focal mechanism of the main shock (after Maeda (submitted)). Diagram is a projection of the upper focal hemisphere with a Wulff net.

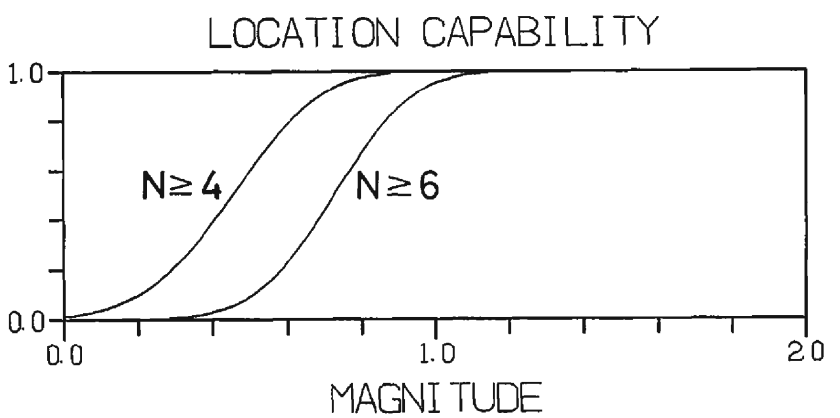

Fig. 3. The location capability curves versus magnitude at the hypocenter of the Kameoka earthquake for the two criteria. *N* represents the number of P times for an earthquake (after Maeda (submitted)).

in **Fig. 4,** the aftershocks are roughly distributed along a westward dipping plane. Maeda (submitted) showed that the fault plane size corresponded to the area where aftershocks occurred within an hour. We fitted a plane to the distribution of aftershocks occurring within an hour by the least squares method. The strike and dip of the plane were estimated to be N6°E and 49°W, respectively. Taking account of the westward dipping aftershock distribution as shown in **Fig. 4,** the nodal plane with a strike of N6°W and a dip of 41°W was regarded as the fault plane of the main shock.

2.4 Seismic activity of the aftershocks

Fig. 5 shows the daily frequency of aftershocks with magnitudes greater than or equal to 1.0. Two prominent peaks of activity occurred on June 2 and 17. The

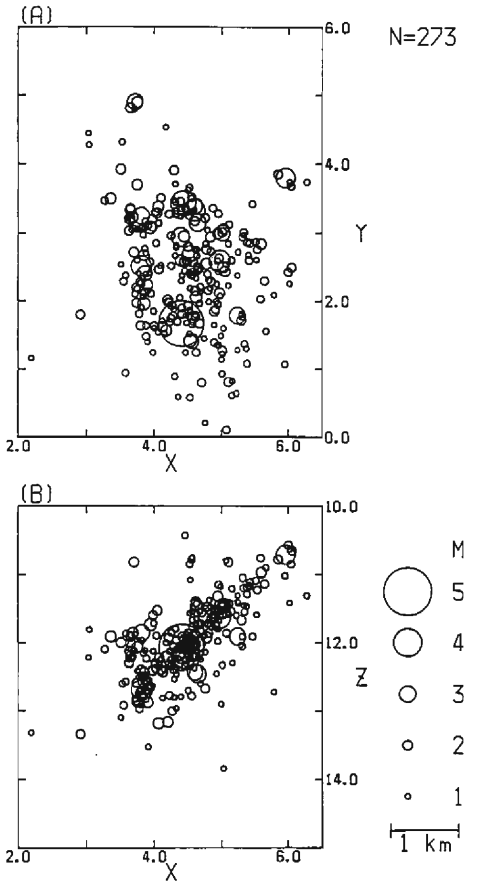

Fig. 4. Epicenter distribution (top) and depth distribution on the east-west vertical plane (bottom) of aftershocks with M 1.0 and greater (after Maeda (submitted)).

aftershocks with M 3.8 and M 3.5 on August 28 and September 1 were the largest and the second largest aftershocks, respectively. The distribution of the aftershocks which occurred until the end of the September is shown in **Fig. 6,** where the coordinate system is based on the fault plane of the main shock with strike and dip of N6°E and 49°W, respectively. A gap can be seen in the neighborhood of the main shock. Maeda (submitted) showed that the size of the fault plane of the main shock corresponded to the gap. The aftershock distributions for several periods are shown in **Fig. 7** to **Fig. 12,** where the coordinate system is the same as that used in **Fig. 6. Figs. 7, 8, 9, 10, 11,** and **12** show the distributions of aftershocks which occurred within an hour, during May, from June 1 to 14, from June 15 to 30, from July 1 to August 28, and from August 29 to September 30, respectively.

Aftershocks occurred along the periphery of the gap within an hour (**Fig. 7**). During May (**Fig. 8**), most of the aftershocks clustered along the periphery of the gap. In June (**Figs. 9** and **10**), the active region of aftershocks migrated north of that found

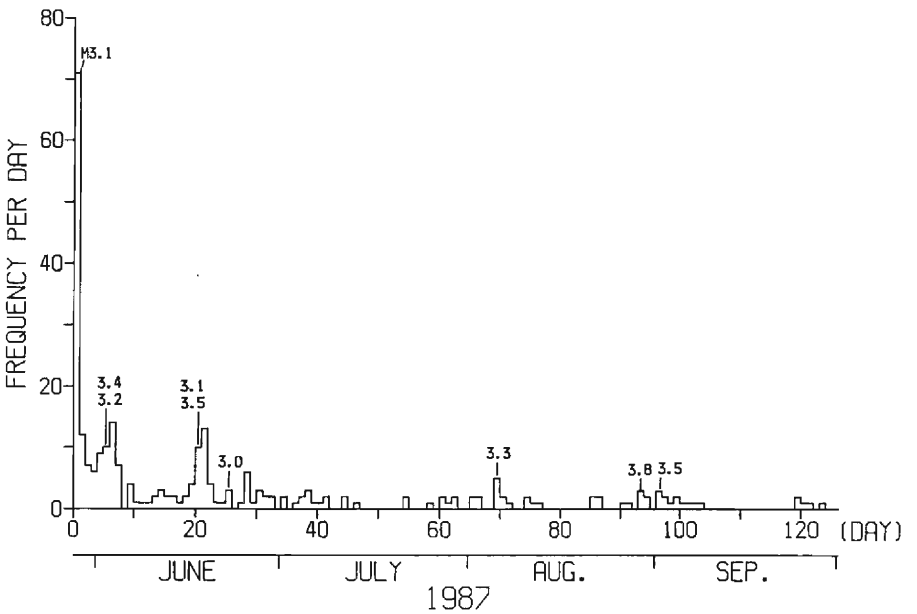

Fig. 5. Daily frequency of aftershocks with M 1.0 and greater (after Maeda (submitted)).

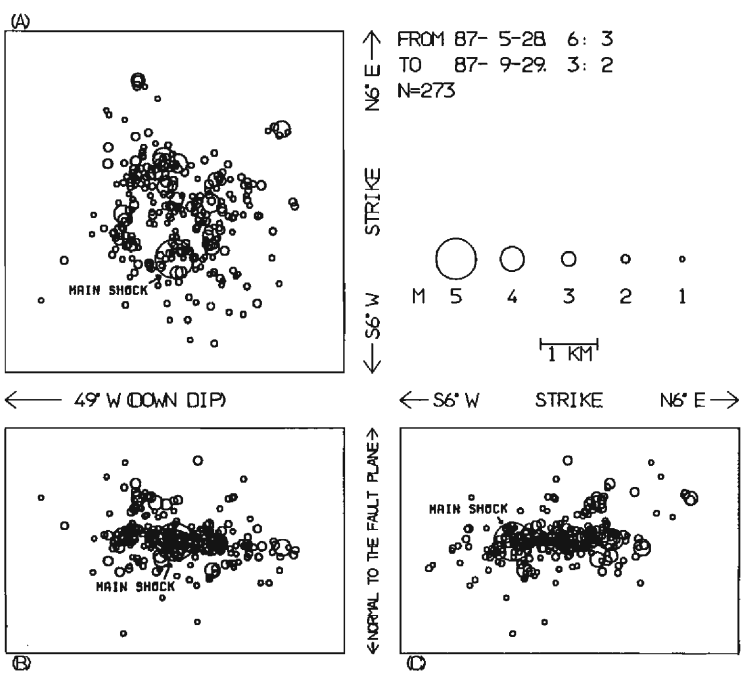

Fig. 6. Distribution of aftershocks which occurred until September 30, 1987. Aftershocks are projected on the planes fixed by the strike, the dip direction, and the normal direction of the fault plane of the main shock.

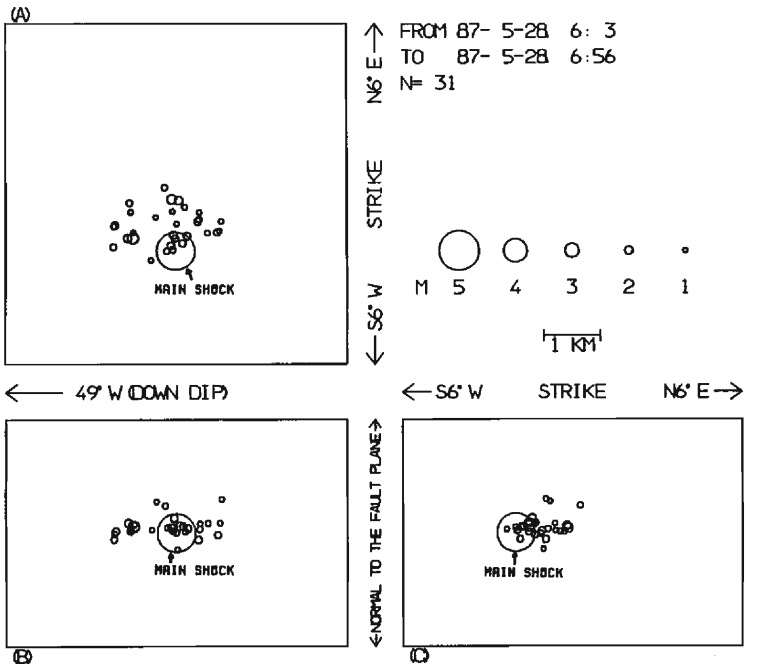

Fig. 7. Distribution of aftershocks which occurred within an hour of the occurrence of the main shock.

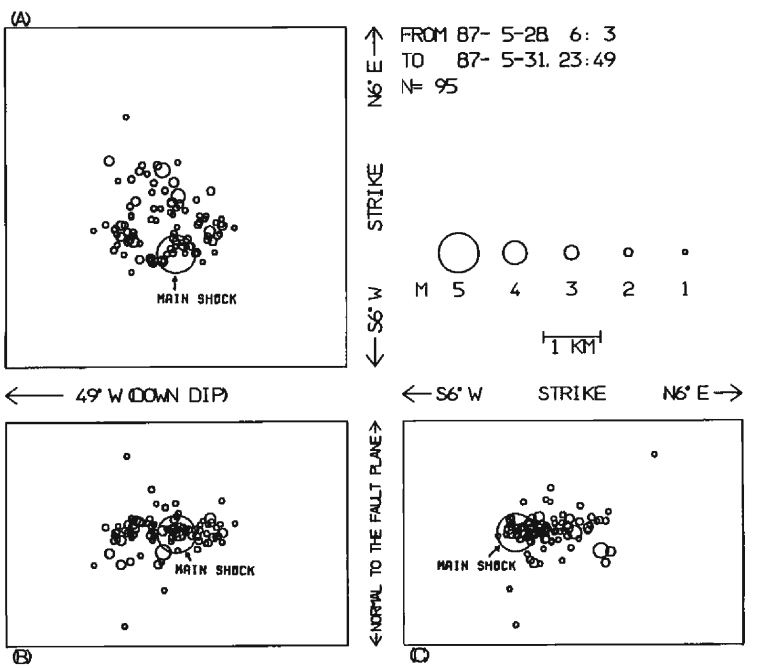

Fig. 8. Distribution of aftershocks which occurred during May 1987.

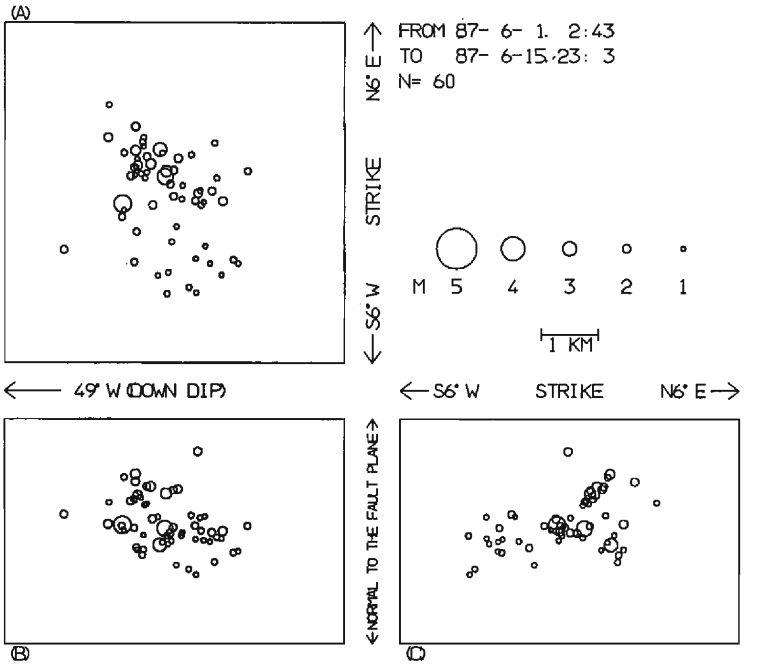

Fig. 9. Distribution of aftershocks which occurred from June 1 to June 14, 1987.

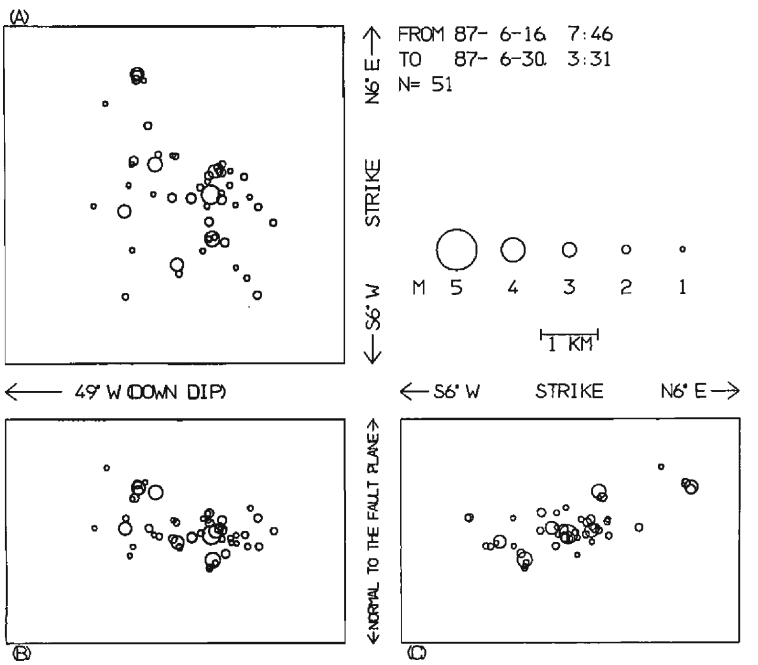

Fig. 10. Distribution of aftershocks which occurred from June 15 to June 30, 1987.

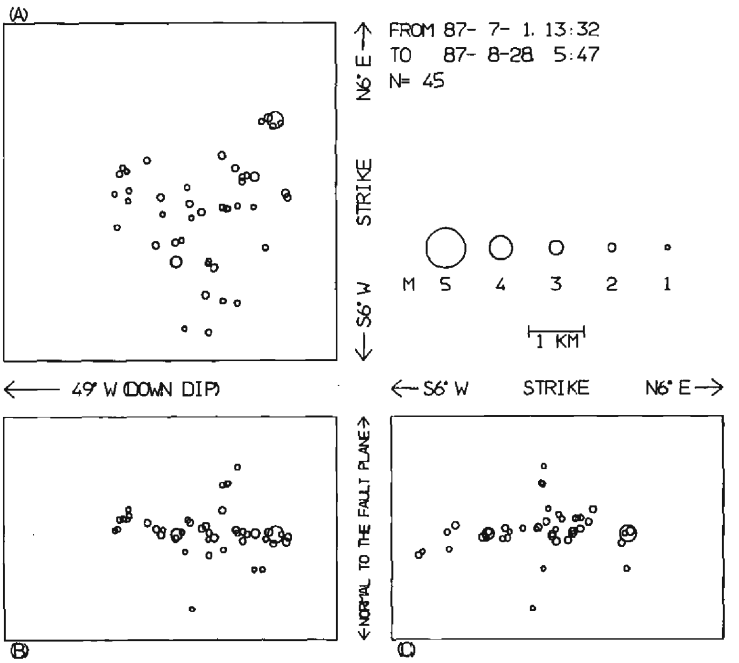

Fig. 11. Distribution of aftershocks which occurred from July 1 to August 28, 1987.

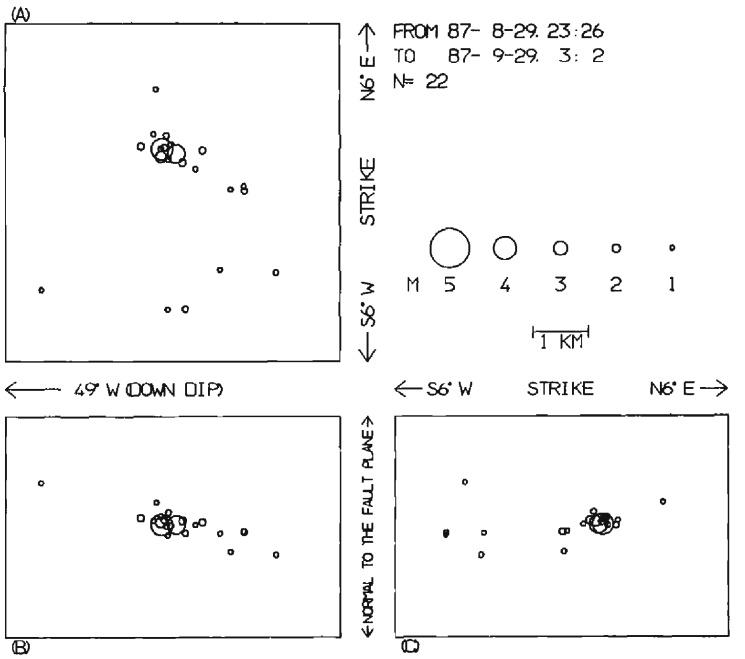

Fig. 12. Distribution of aftershocks which occurred from August 29 to September 30, 1987.

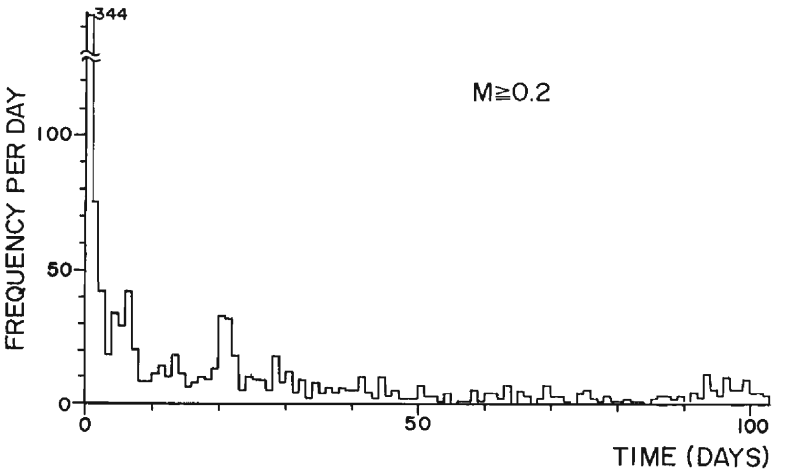

Fig. 13. Daily frequency of aftershocks with magnitudes greater than or equal to 0.2.

in May. In the first half of June (**Fig. 9**), which contained the first peak of activity, aftershocks clustered off the fault plane. In the latter half of June (**Fig. 10**), which contained the second peak of activity, activities off the fault plane decreased in comparison with those in **Fig. 9.** From July 1 to August 28 (**Fig. 11**), the activity was not high. Most aftershocks in this period lay on the fault plane. In the period from August 29 to September 30 (**Fig. 12**), the largest aftershock with M 3.8 and the second largest aftershock with M 3.5 occurred on August 29 and September 1, respectively. These aftershocks occurred on the northern edge of the aftershock area. Overall, the active region migrated northward with time. The aftershocks which occurred near the main shock lay almost on the plane, while the aftershock clusters off the plane were found in the north of the aftershock area. The aftershock distribution seemed bifurcated at the north edge.

Fig. 13 shows the daily frequency of aftershocks with magnitudes greater than or equal to 0.2. The data set used in **Fig. 13** was made in order to investigate the temporal change of b value. In Chapter 4, we will refer to this data set in detail. The distribution of the daily frequency is similar to that in **Fig. 5.** We fitted the modified Omori formula (Utsu, 1961)

$$n(t)=K(t+c)^{-p},\ (K,\ c,\ p:\ \text{parameters}) \tag{1}$$

to this data set, where $n(t)$ and t were the occurrence rate of aftershocks and the lapse time from the main shock, respectively. **Fig. 14** shows $\log n(t)-\log t$ plot. K, p, and c were determined so as to minimize the squares of residuals on $\log n(t)-\log t$ plane. p, c, and K were estimated to be 0.81, 0.005, and 99.9, respectively. The fitted curve is shown in **Fig. 14** as a thin line. As seen in **Fig. 14,** the frequency of the aftershocks seems to be well represented by the modified Omori formula. In order to check the fit of the modified Omori formula to the temporal pattern of aftershock occurrence, the

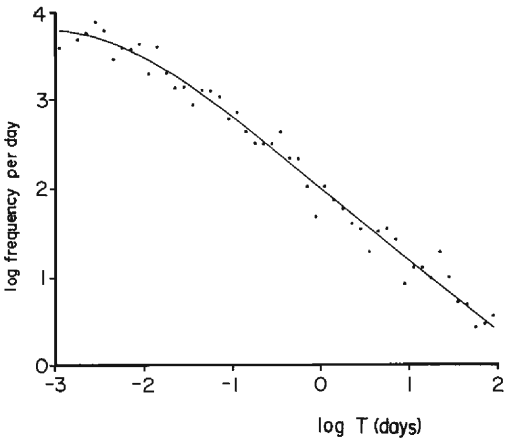

Fig. 14. Rate of aftershock occurrence versus lapse time from the main shock for the Kameoka aftershock sequence.

cumulative number of aftershocks plotted against the frequency–linearized time (Ogata and Shimazaki, 1984) was used. The frequency–linearized time (FLT) is defined as

$$\int_0^t n(s)\,ds, \tag{2}$$

which is equal to the calculated cumulative number of aftershocks using the estimated parameters in (1). If an aftershock sequence is perfectly expressed by (1) with appropriate parameters, the cumulative number of aftershocks increases linearly with FLT. When there is a decrease or increase in activity, the cumulative number plotted against FLT deviates from the straight line (see Matsu'ura, 1986). **Fig. 15** shows the plot of the cumulative number versus FLT for the Kameoka aftershock sequence. An increase in activity above the level expected from the modified Omori formula is found at 20 days. This increase corresponds to the second peak of activity.

3. Stress Tensor Inversion

3.1 Method

The stress tensor inversion is generally based on the assumption that the tangential traction on the fault plane should be parallel to the slip direction (Angelier, 1979, Angelier, 1984, Gephart and Forsyth, 1984). However, the tangential tractions assumed from this assumption may be too small to make fractures occur. The inversion method by Michael (1984) then includes an additional assumption that the magnitude of the tangential traction is similar on the fault planes. Taking account of a fracture criterion, e. g., the Coulomb's fracture criterion, Michael's inversion method is preferable.

When Michael's method is to be applied to focal mechanism data, the fault plane should be chosen out of two nodal planes objectively. Since the inversion is carried out on the assumption of a uniform stress for one data set, we had better find the best

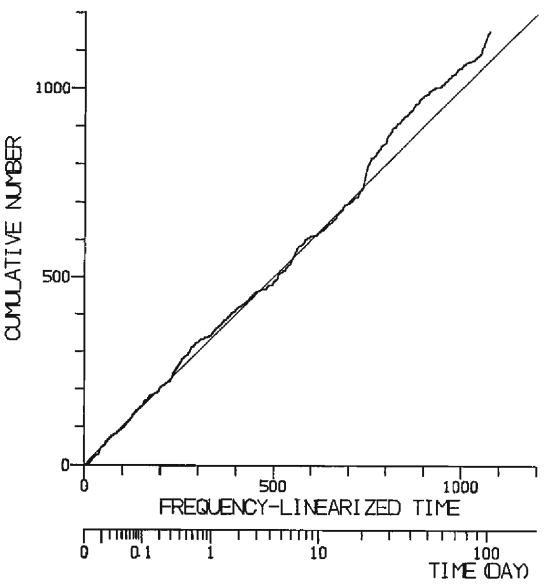

Fig. 15. Cumulative number of aftershocks plotted against the frequency-linearized time.

combination of nodal planes giving the minimum error after the inversions for all combinations of the nodal planes. However, the number of combinations is very large, or 2^N for N focal mechanisms. Computation of the inversion is, therefore, impossible to do practically. As a resolution of this difficulty, a grid search method (Gephart and Forsyth, 1984) was utilized at the step of the fault plane choice.

In the grid search, the nodal plane with smaller difference between the slip vector direction and the direction of the tangential traction calculated for a stress tensor on a grid is picked up as a fault plane of each focal mechanism in a data set. Therefore, once we find the best fitting stress tensor, the best choice of the fault planes is done automatically. As related above, however, the stress tensor obtained by means of the inversion method on the condition that the tangential tractions are parallel to the slip vector may allow only a small magnitude of the tangential traction on the fault plane. Consequently, it is necessary that the stress tensor be finally determined by means of the linear inversion proposed by Michael (1984). In this paper, the stress tensor was determined by two steps. First, the best 500 stress tensors were picked up by means of the grid search. Second, the stress tensor which gave the minimum error was picked up out of the 500 stress tensors determined by means of the linear inversion for the 500 combinations of the fault planes chosen by means of the grid search.

A stress tensor is expressed by using four parameters. Three of them are related to direction cosines of principal stress and the remaining one is the quantity which represents the shape of the deviatoric stress ellipsoid defined as

$$\Phi=\frac{|\sigma_2|-|\sigma_3|}{|\sigma_1|-|\sigma_3|}, \tag{3}$$

where σ_1, σ_2, and σ_3 are the maximum principal stress, the intermediate principal stress, and the minimum principal stress, respectively.

Confidence limits of the principal stress axes were computed by bootstrap resampling proposed in Michael (1987a). If we have a data set of N focal mechanisms, we need N focal mechanisms picked from the same ensemble to simulate the confidence limits by repeating the stress tensor inversion. Accordingly, we made a new data set by picking N focal mechanisms at random out of the original data set containing N focal mechanisms. This newly resampled data set would, therefore, have some mechanisms repeated twice or more, and some mechanisms would be absent. Taking the effect of mischoice of the fault planes on the stress tensor inversion into account, we picked some fault planes out of the resampled data set at random and they were replaced by their auxiliary planes (Michael, 1987b). The stress tensor was then calculated using this new resampled data set. This process could have been repeated many times. Supposing that the number of repetition is N_R, we have new N_R stress tensors. To define X % confidence limits, we pick X % of N_R stress tensors that are closest to the stress tensor determined by the original data set. X % confidence limits are defined by the region where the principal stress axes for the chosen X % of N_R stress tensors are distributed.

3. 2 Data and Analysis

Maeda (1988) determined 196 focal mechanisms of aftershocks of M 1.0 or more, using the polarities and amplitudes of the P wave first motions of the aftershocks. DATA SET 1 with 194 focal mechanisms was made removing two focal mechanisms whose directions of P axes were considerably different from the mean stress field. Moreover, DATA SET 2 with 126 focal mechanisms was extracted out of DATA SET 1, lying within 0.25km of the fault plane of the main shock. DATA SET 1 and DATA SET 2 were used in the stress tensor inversion. In order to see the temporal stress change, the data set was divided into some windows of 20 focal mechanisms so that each window overlapped its neighboring window by half of the window length.

In the grid search, the directions of the maximum principal stress were put on the grid points in the circle of the equal area projection of the upper focal hemisphere, where the circle had a radius of 10 times that of a grid interval. As for the Kameoka aftershock sequence, P axes of the focal mechanisms lay almost horizontally and pointed almost east or west (Maeda, 1988). In order to reduce the calculation time, the range of search for the maximum principal stress was limited to around east or west and near the horizon.

In this paper, 68.2% confidence limit which would correspond to the standard deviation for normal distribution was obtained. In order to define the 68.2% confidence limit, the bootstrap resampling and the stress tensor inversion were repeated 500 times and then the 341 stress tensors with the highest scalar product with the stress tensor determined by the original data set were picked. Considering the effect of mischoice of the fault planes on the confidence limits, 20% of the fault planes in a resampled data set was replaced by the auxiliary planes.

3.3 Results

The results of the stress tensor inversion for DATA SET 1 are shown in **Table 2.** **Fig. 16** shows σ_1, σ_2, σ_3, and their confidence limits for each window of DATA SET 1.

Table 2. Result of stress tensor inversion for DATA SET 1

Window	Mean time (day)	σ_1		σ_2		σ_3		Φ
		θ	φ	θ	φ	θ	φ	
1	0.027	76	−7	69	−102	26	115	0.30
2	0.111	75	−2	72	−97	24	126	0.29
3	0.366	79	4	53	−94	39	108	0.28
4	1.148	89	5	33	97	57	−86	0.31
5	2.291	85	−1	50	103	71	−92	0.31
6	3.901	89	170	41	79	49	−99	0.34
7	5.180	78	−179	55	83	38	−73	0.24
8	6.635	88	−175	19	89	71	−85	0.31
9	11.520	81	4	40	105	51	−93	0.21
10	14.195	76	−3	72	−98	23	122	0.31
11	18.988	77	−6	88	−96	13	164	0.36
12	22.703	83	9	66	102	25	−97	0.27
13	25.661	87	180	72	−89	18	81	0.30
14	31.686	88	176	60	−93	31	84	0.32
15	42.504	84	−177	60	90	31	−77	0.43
16	53.876	87	−172	79	97	11	−67	0.45
17	77.259	81	−178	57	86	35	−75	0.35
18	86.450	82	175	67	81	24	−77	0.38

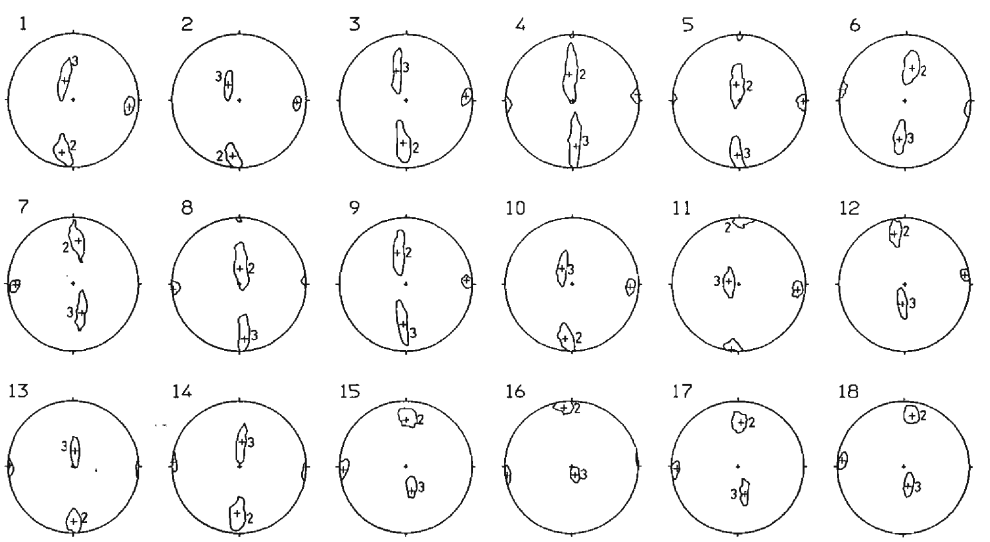

Fig. 16. Results of the stress tensor inversion for DATA SET 1. Principal stress axes with errors are plotted on the upper hemisphere stereonets.

σ_1 is almost horizontal and points either east or west. In such a case, when σ_2 is horizontal, earthquakes with thrust type faulting are apt to occur. When σ_3 is horizontal, earthquakes with strike slip type faulting are apt to occur. Looking at stress tensors from the viewpoint of corresponding faulting type, stress tensors for the first two windows of DATA SET 1 indicate thrust type, while stress tensors for windows 3 to 9 indicate strike slip type or intermediate type. Finally, faulting type returns to thrust type for windows 10 to 18. **Figs. 17** and **18** show the temporal change of σ_1 and σ_2, respectively. In **Fig. 17,** angles were measured after σ_1 was projected on the eastern

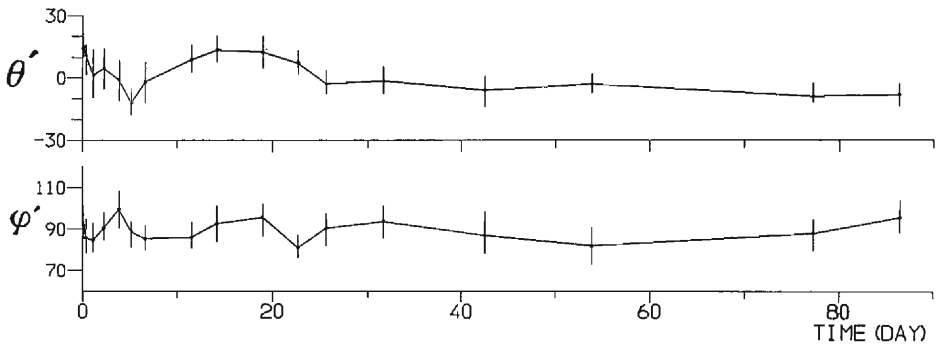

Fig. 17. Temporal change of the maximum principal stress (σ_1) for DATA SET 1. Angles are measured after σ_1 was projected on the eastern hemisphere of the focal sphere. θ' represents the angle from the horizon measured upward and φ' represents the azimuthal angle measured anticlockwise from the east.

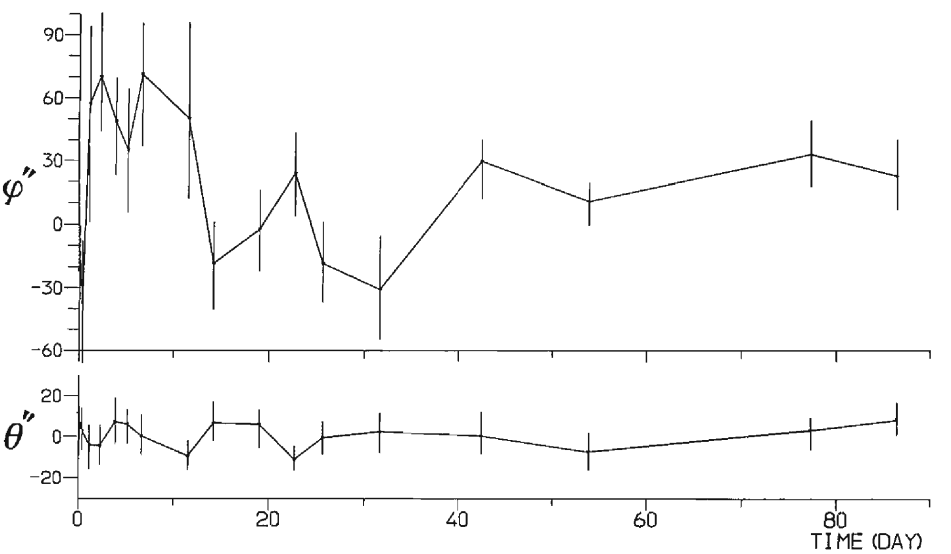

Fig. 18. Temporal change of the intermediate principal stress (σ_2) for DATA SET 1. Angles are measured after σ_2 was projected on the northern hemisphere of the focal sphere. θ'' represents the angle from the vertical plane with a north strike, and φ'' represents the angle between the projections of σ_2 to the vertical plane and the north.

hemisphere of the focal sphere. θ' represents the angle from the horizon measured upward and φ' represents the azimuthal angle measured anticlockwise from the east. In **Fig. 18,** angles were measured after σ_2 was projected on the northern hemisphere of the focal sphere. θ'' represents the angle from the vertical plane with a north strike, and φ'' represents the angle between the projection of σ_2 to the vertical plane and the north. Small bars in **Figs. 17** and **18** represent confidence limits. θ' and φ' of σ_1 fell within $\pm 15^\circ$ and within $\pm 10^\circ$, respectively. These angles were almost constant for the period of the analysis except that θ' of σ_1 within 25 days fluctuated beyond the confidence limits. θ'' of σ_2 fell within $\pm 10^\circ$. φ'' of σ_2 indicated the stress tensors within 12 days where earthquakes with a strike slip type faulting or intermediate type were apt to occur. Temporal change of σ_1 and σ_2 for DATA SET 1 indicated that the stress tensor fluctuated within about 25 days and then approached a constant.

As related in Maeda (1988), most of earthquakes of a strike slip type or an intermediate type occurred off the fault plane. Aftershocks occurring off the fault plane may show different focal mechanism types from that of the main shock since the stress field is disturbed by the faulting during the main shock (e. g., Nishida, 1990). Because DATA SET 1 contained all of the focal mechanisms of aftershocks, the result that stress tensors fluctuated within about 25 days and then became almost constant can be related to the occurrence of earthquakes off the fault plane.

We made DATA SET 2, extracting the aftershocks lying within 0.25km of the fault plane of the main shock, and carried out the stress tensor inversion for this data set. The results are shown in **Table 3. Fig. 19** shows σ_1, σ_2, σ_3, and their confidence limits for each window of DATA SET 2. **Figs. 20** and **21** show the temporal change of σ_1 and σ_2, respectively. The angles, θ' and φ', in **Fig. 20** and, θ'' and φ'', in **Fig. 21** were measured by the same manner as those in **Figs. 17** and **18,** respectively. These figures show that fluctuation of temporal change of σ_1 and σ_2 for DATA SET 2 are smaller than that for DATA SET 1. The stress tensors show that earthquakes with thrust type faulting are apt to occur except Window 5. It seems that σ_1 approaches a certain value

Table 3. Result of stress tensor inversion for DATA SET 2

Window	Mean time (day)	σ_1		σ_2		σ_3		Φ
		θ	φ	θ	φ	θ	φ	
1	0.032	74	−1	75	−96	23	134	0.26
2	0.204	74	−1	74	−96	22	132	0.32
3	1.250	80	3	81	−89	14	138	0.38
4	2.902	86	−2	85	−92	6	127	0.17
5	8.656	86	−174	45	92	46	−80	0.33
6	13.345	89	6	65	−84	25	98	0.38
7	21.239	90	−176	77	−86	13	94	0.30
8	29.519	86	−179	87	90	5	−43	0.38
9	41.391	81	−178	78	90	15	−51	0.45
10	53.974	81	−175	77	93	16	−51	0.46
11	79.941	81	174	70	81	22	−73	0.38

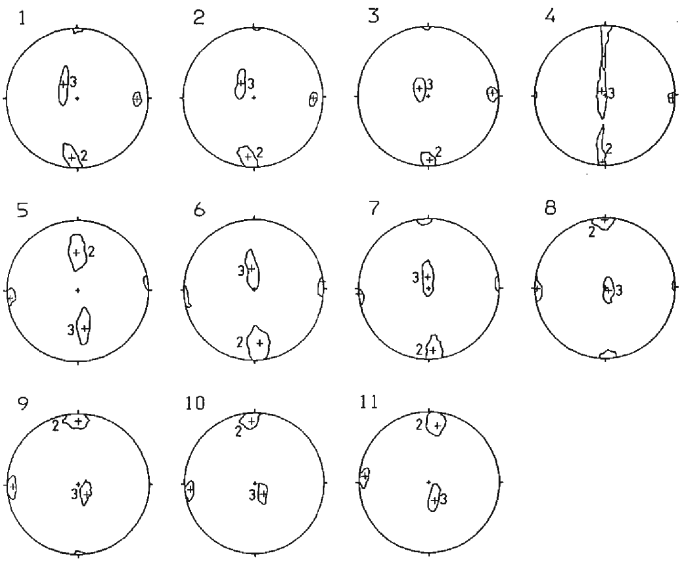

Fig. 19. Results of the stress tensor inversion for DATA SET 2.

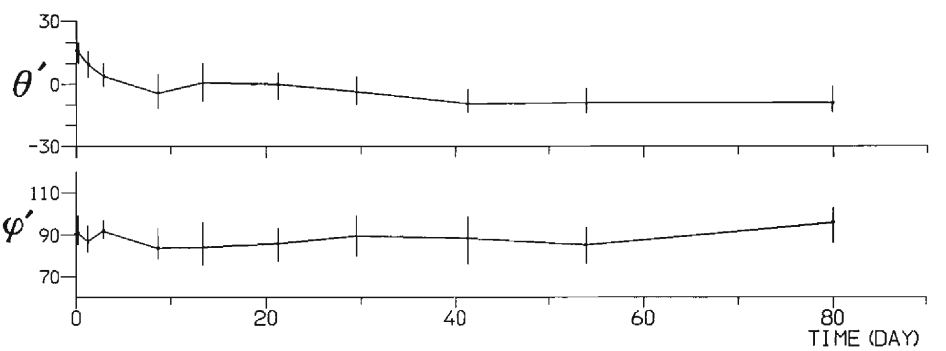

Fig. 20. Temporal change of the maximum principal stress (σ_1) for DATA SET 2. The angles used here represents the same as those used in Fig. 17.

exponentially with time. σ_2 shows the same tendency as σ_1, although fluctuation of σ_2 is large around 10 days. Fitting the expression including exponential function represented by

$$\theta' = a \exp(-\gamma t) + \theta'_0 \tag{4}$$

to a temporal change of θ' of σ_1 using the least squares method, a time constant, that is, $1/\gamma$ was estimated to be 14 days, where θ'_0 was fixed at $-10°$. The fitted curve is shown in **Fig. 22** as a thin line. It seems that the temporal change of the stress tensor shows the process of recovery of the stress field around the main shock.

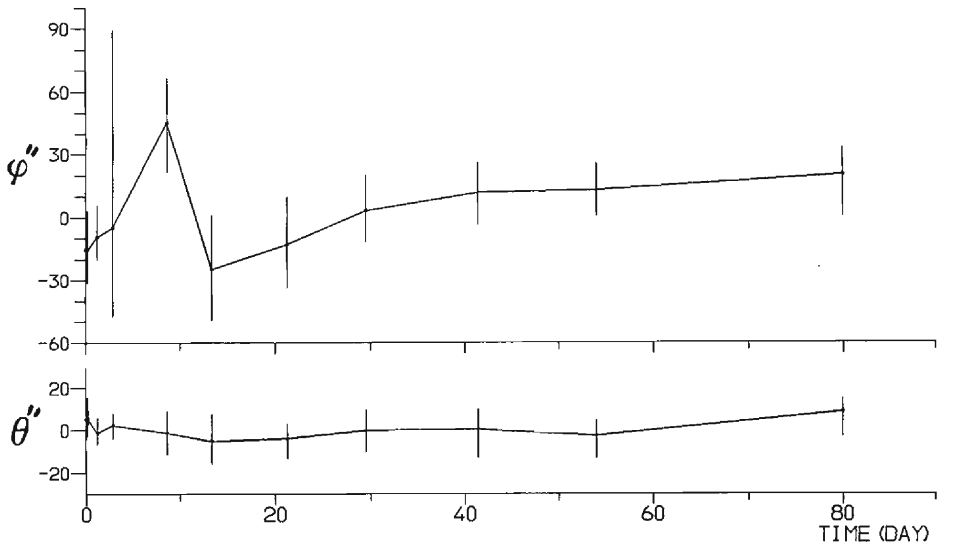

Fig. 21. Temporal change of the intermediate principal stress (σ_2) for DATA SET 2. The angles used here are the same as those used in Fig. 18.

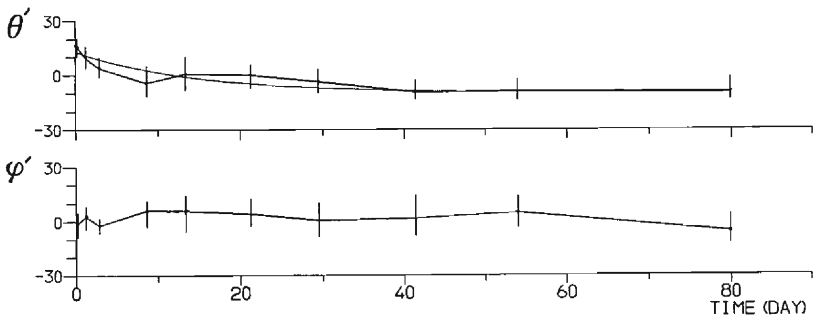

Fig. 22. Temporal change of θ' of σ_1 for DATA SET 2 (thick line) and the curve, expressing equation (4), fit for the temporal change (thin line). A time constant was estimated to be 14 days.

4. Temporal change of *b* values

4.1 Data

A lot of earthquakes are required for the analysis of temporal change of *b* values. We were able to determine the hypocenters of aftershocks with magnitude of about 0.8 or more. 419 aftershocks were located from the occurrence of the main shock to the end of September, 1987. This number, however, was too small to discuss the temporal change of *b* values. Seismic waves are recorded at ASO on magnetic tape when events are detected, and events on magnetic tape are routinely processed for picking phase times and determination of hypocenters. In addition, for the purpose of watching the condition

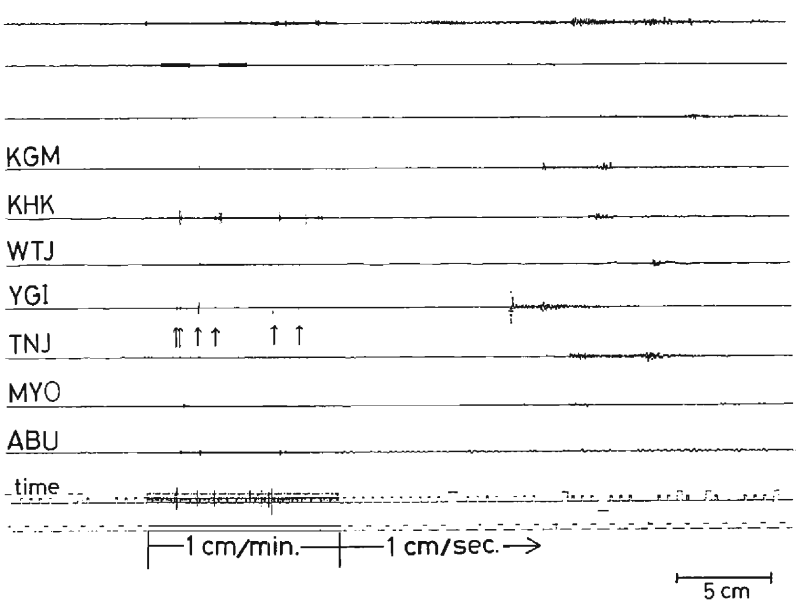

Fig. 23. A part of thermal pen recorder tracings. Paper speed is usually 1cm/minute, and 1cm/second when events are detected. Many of the aftershocks following the Kameoka earthquake are found in the slower part of traces.

of seismographs and telephone lines, seismic signals are always monitored with a thermal pen recorder. We utilized the traces on the thermal pen recorder in order to increase the mumber of aftershocks. The paper speed of the traces is usually 1cm/minute, and 1 cm/second when events are detected. As shown in **Fig. 23,** many of the aftershocks following the Kameoka earthquake can be seen in the slower part of traces, but we can not pick the phase time of these small earthquakes with enough accuracy to determine hypocenters. We recorded seismic signals continuously on magnetic tape for 18 hours from one hour after the main shock, and compared the wave forms of small aftershocks on magnetic tape with those on paper in order to train for recognizing the pattern of the aftershocks following the Kameoka earthquake. We picked up small aftershocks on the traces of seismic signals observed at the seven stations when possible. The criterion for selection of aftershocks is that the maximum amplitude at YGI, which is the nearest station to the hypocenter of the main shock, is 1mm or more on paper. In this way, we were able to made a data set with 2136 aftershocks by adding the aftershocks picked up from the slower part of the traces on the thermal pen recorder to the aftershocks picked up routinely.

4. 2 Magnitude

Magnitudes of aftershocks were determined using maximum amplitudes. For this purpose, hypocenter locations were required. It was, however, impossible to locate hypocenters of small aftershocks picked up from the slower part of the traces. We therefore assumed the hypocenter of small aftershocks as the center of the aftershock

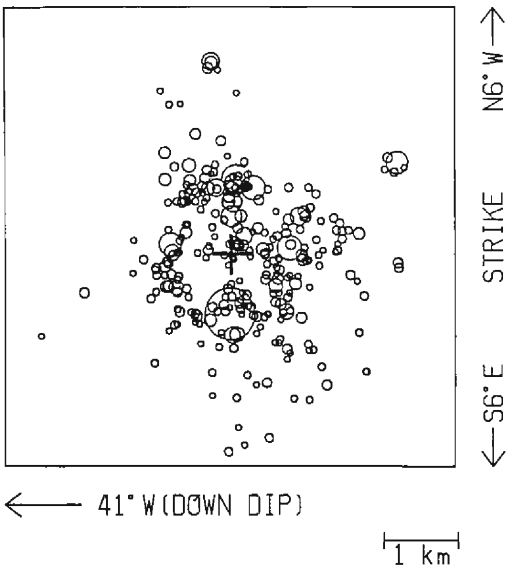

Fig. 24. Assumed hypocenter for magnitude determination of small aftershocks found in the slower tracings. It is represented by a cross.

distribution, which was represented by a cross in **Fig. 24.** Suppose that the real hypocenters of small aftershocks lie in the area where aftershocks concentrate, the error of magnitude caused by assuming the hypocenter location is estimated to be within 0.1.

In determination of magnitude, we used station corrections for the aftershock sequence as follows. First, magnitude for each station was determined using Watanabe's formula (Watanabe, 1971) with the station correction obtained by Maeda (1984). At this time, the assumed hypocenter was used for the small aftershocks picked up from the traces on paper, and the hypocenter determined routinely was used for the aftershocks recorded on magnetic tape. Second, magnitude of an aftershock whose maximum amplitudes were picked up from the seven stations, was determined by averaging the magnitudes from the seven stations. Third, a residual of magnitude for each station was calculated. Finally, a station correction for each station was obtained by averaging the residuals of the stations. Using these station corrections, magnitudes of the aftershocks picked up from the traces on paper and the aftershocks selected routinely were determined.

Fig. 25 shows the magnitude-frequency plots for aftershocks following the Kameoka earthquake. As seen in **Fig. 25,** we were able to pick up the aftershocks with magnitudes of 0.2 or more consistently.

4.3 Result

In order to calculate b values, we made a new data set extracting the aftershocks with magnitudes as small as 0.2. The data set was divided into several windows of 200 aftershocks so that each window overlapped its neighbor by seven eighths of the window

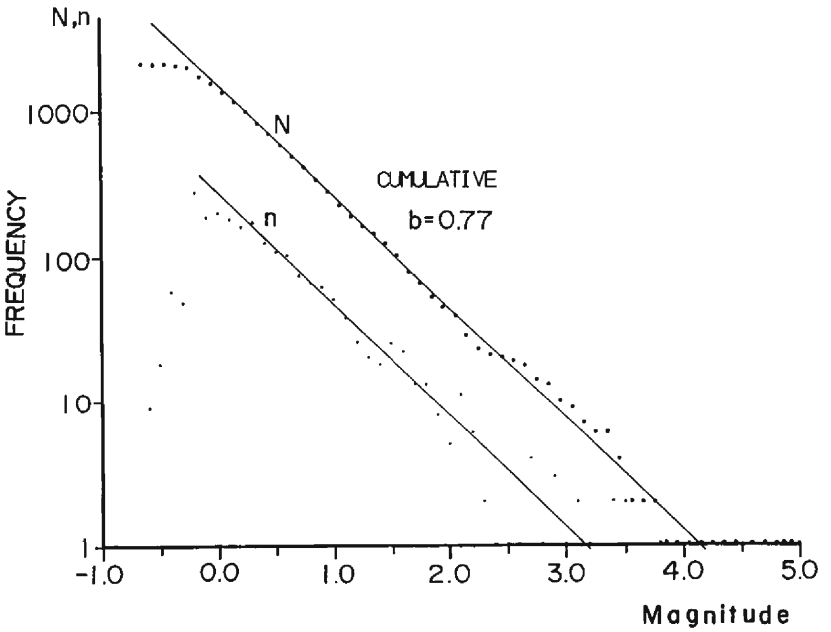

Fig. 25. Magnitude–frequency plots for aftershocks following the Kameoka earthquake. The aftershocks with magnitudes of 0.2 or more were picked up consistently.

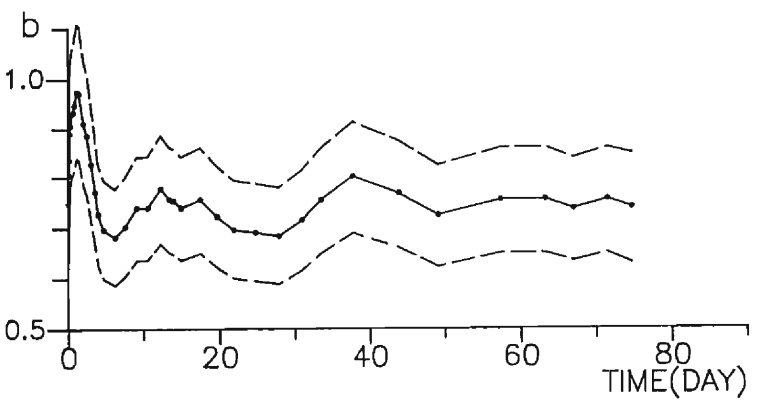

Fig. 26. The temporal change of b value (solid line) and 95% confidence limits (broken line).

length. b values were calculated using the maximum likelihood estimate (Utsu, 1965; Aki, 1965). **Fig. 26** shows the temporal change of b values. 95% confidence limits of b values (Aki, 1965) fall in the range 0.09 to 0.13. b values within five days after the main shock are significantly large taking account of the confidence limits, and then they approach about 0.75 with time. For earthquakes which occurred in the area shown in **Fig. 4** from January 1976 to April 1987, b value was estimated to be 0.8 as shown in **Fig. 27.** Accordingly, it was verified that b values during the aftershock sequence became

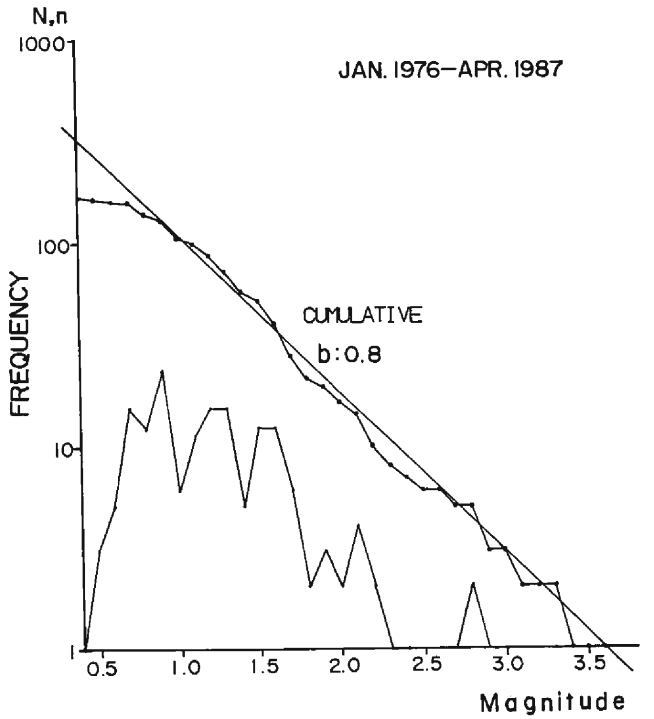

Fig. 27. Magnitude–frequency plots for earthquakes which occurred in the area shown in Fig. 4 from January 1976 to April 1987. *b* value is estimated to be 0.8.

large immediately after the main shock and finally approached almost the same value as the stationary one in the area around the main shock.

5. Discussion

The rotation of the maximum principal stress which was found using the stress tensor inversion was reported for the aftershock sequences of the 1983 Coalinga earthquake (1983, $M_L=6.7$) (Michael, 1987b) and the 1986 Oceanside earthquake (1986, $M_L=5.3$) (Hauksson and Jones, 1988). There is a difference between the rotation reported by them and the rotation for the Kameoka aftershock sequence. The rotation reported by them was an azimuthal temporal change, while it is a rotation about a north–south axis for the Kameoka aftershock sequence. Michael (1987b) suggested that the rotation was attributable to the decay of the stress anomaly caused by the main shock. Hauksson and Jones (1988) regarded the anomaly as the stress drop in the focal area. However, the aftershocks immediately after the main shock occurred at the periphery of the fault plane of the main shock, where the stress level was high due to the main shock faulting. Consequently, the stress anomaly should not be regarded as a stress decrease, but stress concentration. Mogi (1967) pointed out that the high stress level immediately after the main shock and the decay process of the stress level were required to explain

the curve representing the frequency of aftershock per unit time. From this reasoning, it is considered that the curve of the stress rotation is related to the decay process of the stress level.

To produce a rotation, all that is required is that the stress change has different principal axes than the original stress field. As regards the Kameoka earthquake, eight focal mechanisms were obtained out of 11 earthquakes which occurred in the neighborhood of the aftershock area within 6 months before the main shock. Although the number of the focal mechanisms was insufficient for the stress tensor inversion, we tried to do the inversion using these focal mechanisms. As a result, θ' was estimated at $-3.3°$. Looking at **Fig. 22** this value is closer to θ_0' than to θ' at $t=0$. Although the value contains large error because of the small number of the focal mechanisms used in the stress tensor inversion, this result is enough to suggest that the main shock produced stress change which had different principal axes than the original stress field.

The time constant for the decay would be helpful in understanding the physical mechanism of the decay process. Michael (1987b) and Hauhsson and Jones (1988) did not obtain time constants for respective sequences, to which Michael attributed the large errors in the azimuths, as well as the difficulty in assigning a single physically meaningful time to each window. It is, however, possible to roughly estimate the time constant, or at least to obtain its order. Picking the time constants from their figures which show the azimuthal rotation change, the time constants are estimated to be about 15 days for the Coalinga aftershock sequence and about 5 days for the Oceanside aftershock sequence. The time constant for the Kameoka sequence was estimated to be 14 days. These values are of the same order and seem to be independent of earthquake magnitude.

When the decay process is simply regarded as the stress relaxation of the Maxwell body under constant strain, the viscosity is estimated as the product of rigidity and relaxation time constant. Assuming the velocity of S wave, and the density of crustal rocks to be 3.5 km/s and 2.6 g/cm^3, respectively, the viscosity is estimated to be 3.8×10^{17} P. This valus is too small for the viscosity of crustal rocks. These estimations, therefore, suggest that a time constant of 14 days is for a process that is much faster than the large scale tectonic deformation of the crust. Nur and Booker (1972) proposed a model for aftershock occurrence based on decrease of strength due to pore fluid flow. They concluded that the time constant associated with the pore pressure decay most likely ranged from several hours to several months. The time constant for the Kameoka aftershock sequence falls in this range. In this model, the flow of water is necessary. The migration of the aftershock activity in the Kameoka aftershock sequence implies the existence of a flow. The time constant for the Kameoka aftershock sequence may be explained by such a pore fluid flow model.

The result of the stress tensor inversion for DATA SET 1 showed that the stress field within 12 days was the field where earthquakes with a strike slip or intermediate type faulting tended to occur. This tendency was not found in the result for the DATA SET 2. These results are reasonable, because the aftershocks which occurred off the fault plane were eliminated in DATA SET 2. The focal mechanisms of aftershocks were influenced by the disturbance of stress field caused by the main shock faulting (e. g.,

Nishida, 1990). Therefore, the focal mechanisms found off the fault plane indicated a different faulting type from that of the main shock. In the time series of aftershock activity, two prominent peaks were found. As related in Chapter 2, an increase in activity above the level expected from the modified Omori formula was found at 20 days. This increase corresponds to the second peak of activity. The time constant of 14 days lies between the two peaks. The time constant of the stress rotation, the period of the occurrence of the aftershocks with strike slip faulting or intermediate faulting type, and the period in which the modified Omori formula held are thought to be the same, taking errors in determination of the respective values into account. This fact suggests that the aftershocks with strike slip or intermediate faulting type occur when the stress magnitude is still large, and that the modified Omori formula holds well during this period.

In the case of the Kameoka aftershock sequence, the b value was meaningfully large within five days after the main shock, as shown in **Fig. 23.** Most of the aftershocks in this period occurred at the edge of the fault plane, or in the regions where the stress level was highest due to main shock faulting. The hypocenters of the small aftershocks used in the analysis of the temporal change of b values could not be determined, but it was natural that such small aftershocks were assumed to occur in the same region as the larger aftershocks occurred. Scholz (1968) related a large magnitude of differential stress with a small b value from his experimental results. According to his result, large b values found after the main shock indicated decrease of stress in the focal area. As regards the Kameoka aftershock sequence, this idea does not hold because large b values are found under high stress levels. Mogi (1962) related a large b value with a large degree of heterogeneity of the medium. Regions around the edge of the fault plane can be damaged by the motion during the main shock faulting and the heterogeneity around the edge is thought to be extensive. Therefore, the large b values within 5 days after the main shock may be attributed to the large degree of heterogeneity of the medium where aftershocks occurred in cluster.

6. Conclusions

The temporal change of the stress tensors estimated using focal mechanisms and the temporal change of Gutenberg–Richter's b value were investigated for the aftershock sequence following the Kameoka earthquake. The results are summarized as follows:

(1) The rotation of the maximum principal axis of the stress tensor was found. The rotation shows exponential change with a time constant of 14 days. Taking the reports on the rotation of stress axis in the cases of the Coalinga and the Oceanside earthquakes into consideration, these time constants are estimated to be about 10 days and seem to be independent of the magnitude of the main shock.

(2) It was revealed that this time constant was almost the same as the period of occurrence of the aftershocks with strike slip faulting or intermediate faulting type which was different from that of the main shock. The time constant corresponded also to the period where the modified Omori formula held well. This fact shows that the various types of faulting are apt to occur in the period where the stress level is still high.

(3) Meaningfully large b values were found within five days after the main shock when the aftershocks were occurring along the periphery of the fault plane of the main shock where the stress level was high. It is verified that the large b values found in rock experiments under the relatively low stress levels do not correspond to the temporal variation of b values in the aftershock sequence.

Acknowledgements

The authors would like to express their appreciation to Drs. A. J. Michael and Y. Ogata for their useful suggestions. Thanks are extended to the members of the staff of the Abuyama Seismological Observatory, Kyoto University for their helpful discussions. The authors thank Drs. K. Kohketsu and K. Takano for use of the emulation software, ETERM.

REFERENCES

Aki, K., Maximum likelihood estimate of b in the formula log $N=a-bM$ and its confidence limits, Bull. Earthq. Res. Inst., Univ. Tokyo, **43,** 237–239, 1965.

Angelier, J., Determination of the mean principal direction of stresses for a given fault population, Tectonophysics, **56,** T17–T26, 1979.

Angelier, J., Tectonic analysis of fault slip data sets, J. Geophys. Res., **89,** 5835–5848, 1984.

Gephart, J. W. and D. W. Forsyth, An improved method for determining the regional stress tensor using earthquake focal mechanism data : Application to the San Fernando earthquake sequence, J. Geophys. Res., **89,** 9305–9320, 1984.

Gutenberg, B. and C. F. Richter, Frequency of earthquakes in California, Bull. Seismol. Soc. Am., **34,** 185–188, 1944.

Hauksson, E. and L. M. Jones, The July 1986 Oceanside (M_L=5.3) earthquake sequence in the continental borderland, south California, Bull. Seismol. Soc. Am., **78,** 1885–1906, 1988.

Ito, K. and A. Kuroiso, Detailed spatial distributions of foreshock and aftershock activities of small earthquakes, Zisin 2, **32,** 317–327, 1979 (in Japanese with English abstract).

Kuroiso, A. and H. Watanabe, On the telemetered array system for microearthquake observation at Abuyama Seismological Observatory, Zisin 2, **30,** 91–106, 1977 (in Japanese with English sbstract).

Maeda, N., On accuracy of magnitude determination—in case of maximum velocity amplitude magnitude—, Zisin 2, **37,** 310–313, 1984 (in Japanese).

Maeda, N., Method for computing focal mechanisms for an earthquake cluster—Aftershocks of the earthquake with M 4.9 occurred in Kyoto–Osaka border region on May 28, 1987—, Zisin 2, **41,** 323–333, 1988 (in Japanese with English abstract).

Maeda, N., Comparison of the aftershock distribution and the fault plane size of the M 4.9 Kameoka earthquake on 28 May, 1987, Japan, submitted to Tectonophysics.

Maeda, N. and H. Watanabe, Mode of activity of microeathquakes —In the case of the middle and northern part of Kinki District, Southwestern Japan—, Zisin 2, **37,** 579–598, 1984 (in Japanese with English abstract).

Matsumura, S., Evaluation of detection capability of microearthquakes for an observational network, Zisin 2, **37,** 474–489, 1984 (in Japanese with English abstract).

Matsu'ura, R. S., Precursory quiescence and recovery of aftershock activities before some large aftershocks, Bull. Earthq. Res. Inst., Univ. Tokyo, **61,** 1–65, 1986.

Michael, A. J., Determination of stress from slip data : faults and folds, J. Geophys. Res., **89,** 11517–11526, 1984.

Michael, A. J., The use of focal mechanisms to determine stress : A control study, J. Geophys. Res., **92,** 357–368, 1987a.

Michael, A. J., Stress rotation during the Coalinga aftershock sequence, J. Geophys. Res., **92**, 7963–7979, 1987b.

Mogi, K., Study of elastic shocks caused by the fracture of heterogeneous materials and its relation to earthquake phenomena, Bull. Earthq. Res. Inst., Univ. Tokyo, **40**, 125–173, 1962.

Mogi, K., Earthquakes and fractures, Tectonophysics, **5**, 35–55, 1967.

Nishida, R., Characteristics of the 1983 Tottori earthquake sequence and its relation to the tectonic stress field, Tectonophysics, **174**, 257–278, 1990.

Ogata, Y. and K. Shimazaki, Transition from aftershock to normal activity : the 1965 Rat Islands earthquake aftershock sequence, Bull. Seismol. Soc. Am., **74**, 1757–1765, 1984.

Scholz, C. H., The frequency–magnitude relation of microfracturing in rock and its relation to earthquakes, Bull. Seismol. Soc. Am., **58**, 399–415, 1968.

Utsu, T., A statistical study on the occurrence of aftershocks, Geophys. Mag., **30**, 521–605, 1961.

Utsu, T., A method for determining the value of b in a formula log $n=a-bM$ showing the magnitude–frequency relation for earthquakes, Geophys. Bull. Hokkaido Univ., **13**, 99–103, 1965 (in Japanese).

Watanabe, H., Determination of earthquake magnitude at regional distance in and near Japan, Zisin 2, **24**, 189–200, 1971 (in Japanese with English abstract).

Watanabe, H., A. Kuroiso, and N. Maeda, A fully automatic microearthquake observation system at the Regional Center for Earthquake Prediction, Kyoto University (in preparation).